Active suppression of microphonics detuning in high Q_L cavities

Nilanjan Banerjee,* Georg Hoffstaetter, Matthias Liepe, Peter Quigley, and Zeyu Zhou
Department of Physics, Cornell University, Ithaca, New York 14853, USA

(Received 26 November 2018; published 9 May 2019)

Operation of superconducting radio frequency (SRF) cavities with high loaded quality factors is becoming increasingly preferred for applications which involve low beam loading including energy recovery linacs (ERL). Vibration induced microphonics detuning poses a major operational bottleneck in these low bandwidth systems, adversely affecting field stability. Besides passive measures of mitigating the vibration sources, modern SRF cavities are also attached to fast tuners incorporating piezoelectric actuators. We demonstrate the narrow band active noise control algorithm for realizing active resonance control and propose a modification based on the least mean square approach to adaptively tune the control parameters and study its stability and performance. We discuss our experience of using passive mitigation techniques while commissioning the main linac cryomodule of the Cornell-BNL ERL test accelerator and report a net reduction in peak detuning by more than a factor of 2 in its unstiffened cavities. Finally, we demonstrate stable performance of our resonance control system with consistent reduction of peak microphonics detuning by almost a factor of 2 on multiple cavities.

DOI: 10.1103/PhysRevAccelBeams.22.052002

I. INTRODUCTION

Modern particle accelerators are reaching the pinnacle of efficiency using superconducting radio frequency (SRF) cavities which are characterized by low loses arising from high intrinsic quality factors ($Q_0 \gtrsim 10^{10}$) [1]. The microwave power requirements of such SRF cavities depend on the effective beam loading and the loaded quality factor Q_L used in operation. In situations of high beam loading, they are operated with a comparatively low Q_L in order to couple the required power into the beam, such as in the LHC [2], CESR [3], NSLS-II [4] and many others. However, in new applications such as light source linacs (e.g., LCLS-II [5], XFEL [6]) and in energy recovery linacs (e.g., Cornell-BNL ERL test accelerator (CBETA) [7], bERLinPro [8]), high Q_L is becoming common due to the low or negligible beam loading involved. Low beam loading implies the reduction of the rf power requirements and allows the use of efficient solid state amplifiers.

However, the limited bandwidth arising from large Q_L makes rf systems more sensitive to detuning when operating at a fixed frequency, as during linac operation. Transient changes in the resonant frequency of the cavity resulting from mechanical deformations change its response to the microwaves coming through the fundamental power coupler. Due to enhanced reflection of the incoming waves from a detuned cavity, more power is needed to maintain a stable field. The interaction of the field with the wall currents is one mechanism leading to mechanical deformation and is known as Lorentz force detuning (LFD). This leads to transient detuning as a function of the field inside the cavity and is important for pulsed rf systems. Vibrations inside cryomodules couple into the cavity walls causing transient deformations in its shape resulting in microphonics detuning. The rf power P consumed by a detuned cavity to maintain a voltage V with zero beam loading is given by [9]

$$P = \frac{V^2}{8\frac{R}{Q}Q_L}\frac{\beta+1}{\beta}\left[1+\left(\frac{2Q_L\Delta\omega}{\omega_0}\right)^2\right], \tag{1}$$

where Q_L is the loaded quality factor, β is the coupling factor, R/Q is the shunt impedance in circuit definition and $\Delta\omega$ is the detuning of the SRF cavity. Hence, the maximum voltage which can be stably sustained in a cavity depends on the peak microphonics detuning and is constrained by the peak forward power available from the amplifiers.

Suppression of peak detuning is important in machines operating with high Q_L especially in multiturn ERLs such as CBETA, where there are tight tolerances on field stability (rms amplitude stability of 1×10^{-4} and phase stability of 0.1°) to preserve the intrinsic energy spread of the beam. Designing cavities mechanically less sensitive to vibrations is one way of achieving this goal. Cavities fabricated with metal rings welded onto them can be designed to be less sensitive to vibrations. Depending on

*nb522@cornell.edu

whether the machine will be pulsed or cw, the shape and location of the stiffening rings may be optimized to reduce the effect of LFD or increase its stiffness towards external forces respectively [10]. In this paper, we discuss suppression of the vibration sources and describe active compensation of microphonics detuning to reduce peak power consumption.

In the next section, we describe the design and operation of fast tuners while modeling them as a linear time invariant system and further explore their nonlinear behavior. Using the linear model, we develop a least mean square (LMS) control system based on narrow band active noise control to command the piezoelectric actuators and analyze its performance and stability. Next, we catalog the microphonics sources we found while commissioning the main linac cryomodule (MLC) used in CBETA and the measures we took to mitigate them. We then report on the results of using the active control algorithm during rf operations. Finally, we present a summary of our work and propose some improvements to the resonance control system.

II. FAST TUNER

Mitigation of vibration sources is the preferred method of suppressing microphonics, however an active resonance control mechanism is equally important. By further reducing peak detuning, it improves the margin of power consumption with respect to the maximum capability of the microwave amplifier. It also provides an emergency mitigation mechanism against new sources of microphonics until they are found and suppressed. Active control of microphonics requires the use of fast tuners with acoustic response time scales such as the one used in CBETA [11]. While a stepper motor drives the slow movement of the tuner over a large range, the piezoelectric actuators drive fast movement with a range of 2 kHz [12] which is almost 100 times the operating bandwidth of the cavity. The response of the cavity resonance frequency to voltages applied to the actuator greatly influences the design of the active resonance control system.

A. Linear response

A linear time invariant (LTI) response model can be used to describe the dynamics of the tuner for small excitations of the piezoelectric actuator. In the time domain, the change in resonant frequency $\delta f_{\text{tuner}}(t)$ of the cavity may be written as a convolution of the actuator voltage $u_{\text{pz}}(t)$ with an impulse response function $\tau(t)$ as follows:

$$\delta f_{\text{tuner}}(t) = \int_0^t \tau(t-t')u_{\text{pz}}(t')\mathrm{d}t'. \tag{2}$$

Applying the Fourier transform on both sides of this equation we obtain

$$\delta\tilde{f}_{\text{tuner}}(\omega) = \tau(\omega)\tilde{u}_{\text{pz}}(\omega), \tag{3}$$

where $\delta\tilde{f}_{\text{tuner}}(\omega)$ and $\tilde{u}_{\text{pz}}(\omega)$ are the Fourier transforms of detuning and voltage respectively. $\tau(\omega)$ is the frequency domain tuner transfer function which encodes both the amplitude of the response and the phase shift generated by the tuner. We measured the transfer function at each frequency by exciting the actuator using sine waves of different amplitudes. By using the slope of the linear fit of the response phasor as a function of amplitude we effectively subtracted the background microphonics at the frequency of measurement. Using this procedure, we measured the response of the tuner for frequencies between 5 and 300 Hz which corresponds to most of the vibrations in the main linac cryomodule used in CBETA.

The transfer functions measured on three cavities of the main linac in CBETA are shown in Fig. 1. All the transfer functions show a region of flat amplitude and linear phase response in the range of low frequencies up to 30 Hz; this makes the use of simple algorithms like proportional-integral (PI) control feasible for attenuating low frequency microphonics. The large peaks in amplitude correspond to resonances and they are accompanied by large swings in the phase response of the tuner; this limits feedback control at these frequencies. The measurements also verify one of

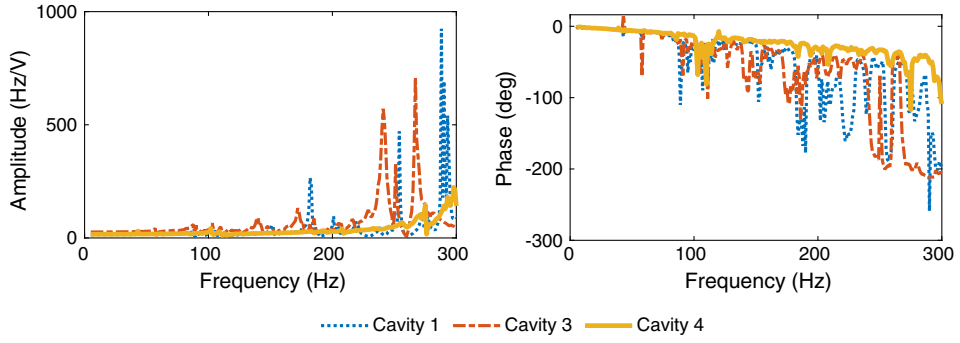

FIG. 1. Tuner response amplitude and phase as functions of excitation frequency for three cavities of the main linac in the CBETA project. The plots show multiple strong resonances above 200 Hz for unstiffened cavities 1 and 3. Cavity 4 is fitted with stiffening rings which suppress the low frequency eigenmodes of the structure.

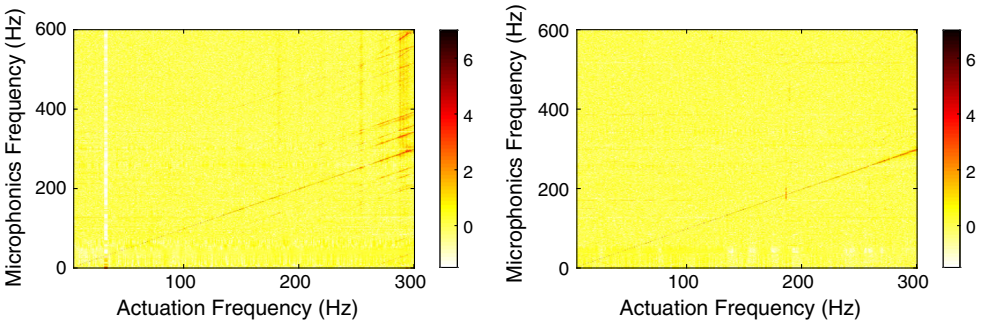

FIG. 2. Spectral response of tuners to single frequency sinusoidal excitations in two cavities of the main linac used in the CBETA project. The plots show the logarithm of power spectra (in color) of tuner response as functions of actuation frequency f_{pz} on the x axes and frequency of detuning f_{detuning} on the y axes. The left and right panels show measurements from an unstiffened and stiffened cavity respectively. The white line on the left panel at the actuation frequency of 30 Hz indicates an absence of valid detuning data due to a rf trip during the measurement.

the design goals of stiffening cavities, shifting the lowest mechanical eigenmode to a higher frequency. The transfer function data can be used to construct a LTI model of the tuner and is used to analyze the stability of the control algorithm used for resonance control.

B. Nonlinear response

The assumption of linearity is dependent on the linearity of the piezoelectric effect, the stress strain curves and damping mechanisms in the materials involved. Although the stress strain curve and the piezoelectric effect are reasonably linear in the regime of use, slight hysteresis is generally observed in resonant frequency as the applied voltage is cycled from 0 V to high voltage back to 0 V [12–14]. This implies that some nonlinearity is present in the system and we should verify its magnitude. A nonlinear response would excite multiple frequencies even if we excite just one [15] and this provides a simple way of diagnosing the nonlinear dynamics of the system by exciting it with sine waves. We measure the power spectrum of detuning for different frequencies of excitation of the tuner and subtract the contribution from the ambient microphonics present in the system to yield an approximate spectral response function.[1] Figure 2 illustrate some examples of spectral responses. The linear response shows up as a line with slope of 1, i.e., the frequency of excitation equals the major frequency component of detuning. However, the plot also shows evidence of higher order responses in the form of additional frequencies in the detuning spectrum.

We can use the straight lines observed in the plots to estimate the order of nonlinearity present in the system and gain some insight into its source. In general, the frequencies present in nonlinear responses of a dynamical system to a sinusoidal excitation can be written as

$$f_{\mathrm{detuning}} = m f_{\mathrm{pz}} + \sum_i n_i f_{\mathrm{vib},i}, \tag{4}$$

where f_{detuning} and $f_{\mathrm{vib},i}$ are the frequencies present in the tuner response and ambient microphonics, while f_{pz} is the frequency of excitation. m and n_i are integers, with $|m|$ representing the order of the nonlinear term and the addition of vibration frequencies represent parametric behavior of the tuner dependent on external microphonics. Both the cavities show lines parallel to the linear response line indicating the presence of modulation from ambient microphonics. The unstiffened cavity further shows the second harmonic with evidence of the $m = 2$ line near $f_{\mathrm{pz}} = 300$ Hz. The strength of the nonlinear responses appear to be a function of frequency with excitation frequencies of above 250 Hz showing the most activity. These observations suggest that we can ignore the nonlinearity as long as we excite the tuner below 250 Hz which limits the bandwidth of the compensation system.

III. ACTIVE NOISE CONTROL

Microphonics compensation of SRF cavity detuning using fast tuners has been demonstrated using a variety of techniques. Resonance control of cw rf cavities typically relies on feedback of microphonics detuning. In this control topology, the detuning acts as an input to the controller which generates a signal for the piezoelectric actuator which in turn affects the net microphonics detuning thus closing the loop. The transfer function of the tuner system as discussed in the previous section plays an important role in designing the controller. The traditional method of proportional-integral feedback has been demonstrated in various machines [16–18] and is very effective when the phase response of the tuner is a monotonous function of frequency which is typical at lower frequencies ($\lesssim 10$ Hz).

[1]We subtract the contributions from ambient microphonics in Fig. 2 using a scaling relation, $\log(\chi'(f_{\mathrm{pz}}, f_{\mathrm{detuning}})) = \log(\chi(f_{\mathrm{pz}}, f_{\mathrm{detuning}})) - \frac{1}{N}\sum_i \log(\chi(f_{\mathrm{pz},i}, f_{\mathrm{detuning}}))$. $\chi(f_{\mathrm{pz}}, f_{\mathrm{detuning}})$ is the spectral power at frequency f_{detuning} when the tuner is excited with a sine wave of frequency f_{pz}.

At higher frequencies, the tuner cavity system typically has mechanical eigenmodes which introduce steps in the phase response which may possibly lead to positive feedback and instability at even modest gains. Consequently, low pass filters are used to ensure stability of the PI loop but at the cost of reducing the bandwidth. Additional bandpass filters may be used in parallel to attenuate certain frequency bands, however manually adjusting them while ensuring stability is inconvenient. In order to get past this limitation, arbitrary digital control filters can be optimized specifically to compensate for a given microphonics spectrum while taking into account the exact phase response of the tuner. This has been demonstrated on the new LCLS-II cryomodules being tested at FermiLab [19].

In the methods described above, the tuner transfer function and the microphonics spectrum are first measured and the data is processed external to the rf control system and the optimal filter coefficients are then uploaded into the control system. In contrast, adaptive tuning of digital control filters inside the rf system during operations using least mean squares algorithms have also been demonstrated. In traditional LMS, an external reference signal which correlates to microphonics detuning is used as an input to a finite impulse response filter whose coefficients are updated continuously to reduce the mean square of detuning [18]. In a different technique [20,21] based on active noise control (ANC) methods, amplitude and phase of sine waves at different frequencies are adjusted to cancel out microphonics. However, both these methods require prior measurement of the tuner transfer function which may be a function of tuner position [10] and may not stay constant over long periods of time and over multiple pressure or temperature cycles. In this paper, we derive the narrow band ANC technique and propose a modification so that it adapts to the tuner response phase *in situ*.

Microphonics detuning due to narrow band vibration sources can be well approximated by a finite series of sinusoids at different frequencies with slowly changing amplitudes and phases. This motivates the use of an algorithm which works by adjusting the amplitudes of a series of sine and cosine functions in order to reduce the mean square detuning. At a particular frequency ω_m, the ideal phase of the actuator signal θ_m^{pz} is determined by not only the relative phase of external detuning with respect to the internal clock $\theta_m^{\mathrm{micro}}$ of the control system but also the phase response ϕ_m of the actuator. The ideal actuator signal phase given by $\theta_m^{\mathrm{pz}} = \theta_m^{\mathrm{micro}} + \phi_m - \pi$ in principle perfectly cancels the sine wave produced by external vibrations. The phase lag ϕ_m introduced by the tuner can be assumed to be a constant when the frequency of vibrations is far from a mechanical resonance, and used as a compensation parameter in the algorithm. Using the technique of stochastic gradient descent, we derive a set of equations which updates the amplitude and phase of individual sinusoids along with online optimization of the phase parameter ϕ_m at the frequencies of vibration.

A. Derivation

Microphonics from narrow band vibration sources may be represented by a finite series of sinusoids at different frequencies with slowly changing amplitudes and phases. Hence, in the time domain, the actuator voltage $u_{\mathrm{pz}}(t)$ can also be written as a sum of sinusoids $u_m(t)$ with frequencies ω_m and whose amplitude and phase are determined by slowly changing $I_m(t)$ and $Q_m(t)$,

$$u_{\mathrm{pz}}(t) = \sum_m u_m(t) = \sum_m I_m(t)\cos(\omega_m t) - Q_m(t)\sin(\omega_m t). \tag{5}$$

The piezoelectric actuator tunes the cavity in response to this signal, the effect of the tuner being represented as a linear transfer function $\tau(\omega)$. Using a phasor notation for the individual frequencies $\tilde{A}_m(t) \equiv I(t) + iQ(t)$, we can write the total actuator voltage in terms of these phasors as $u_{\mathrm{pz}}(t) = \sum_m u_m(t) \equiv \sum_m \mathrm{Re}\{\tilde{A}_m(t)e^{i\omega_m t}\}$. Using this notation we write the detuning near a particular frequency as a linear response integral,

$$f_m(t) = \mathrm{Re}\left\{\frac{1}{2\pi}\int_{-\infty}^{\infty} d\omega \int_{-\infty}^{\infty} dt' \tilde{A}_m(t') e^{i(\omega_m-\omega)t'}\tau(\omega)e^{i\omega t}\right\}, \tag{6}$$

where we have Fourier transformed the actuator voltage, used Eq. (3) which gives us $f_m(\omega) = \tilde{A}_m(\omega)\tau(\omega)$ and finally applied the inverse Fourier transform to calculate the detuning $f_m(t)$ in the time domain. Since the spectral content of microphonics detuning is assumed to be concentrated around certain frequencies, only parts of the transfer function are relevant in modeling the tuner movements.

Far from resonance, where the amplitude of the response does not strongly depend on frequency, we approximate the tuner transfer function around ω_m as

$$\tau(\omega) \simeq \tau_m^{\mathrm{mod}} e^{-i\{\phi_m^{\mathrm{mod}} + \frac{d\phi}{d\omega}|_{\omega_m}(\omega-\omega_m)\}}, \tag{7}$$

where we expand the phase response up to first order. Since this approximation only applies in the neighborhood of ω_m, we impose the restriction of narrow bandwidth on $u_m(t)$, which implies $|\frac{1}{\tilde{A}_m}\frac{d\tilde{A}_m}{dt}| \ll \omega_m$. Using this model in Eq. (6) and changing the order of integration, we get

$$\begin{aligned} f_m(t) &\simeq \mathrm{Re}\left\{\int_{-\infty}^{\infty} dt' \tilde{A}_m(t') e^{i\omega_m t'} \right. \\ &\quad \left. \times \frac{1}{2\pi}\int_{-\infty}^{\infty} d\omega \tau_m^{\mathrm{mod}} e^{i\{-\phi_m^{\mathrm{mod}} + \frac{d\phi}{d\omega}|_{\omega_m}\omega_m\}} e^{i\omega(t-t'-\frac{d\phi}{d\omega}|_{\omega_m})}\right\} \\ &= \mathrm{Re}\left\{\tau_m^{\mathrm{mod}} e^{i\{-\phi_m^{\mathrm{mod}} + \frac{d\phi}{d\omega}|_{\omega_m}\omega_m\}} \int_{-\infty}^{\infty} dt' \tilde{A}_m(t') e^{i\omega_m t'} \right. \\ &\quad \left. \times \delta\left(t - t' - \left.\frac{d\phi}{d\omega}\right|_{\omega_m}\right)\right\}, \end{aligned} \tag{8}$$

where the integral over ω becomes a delta function which represents the approximate time domain impulse response valid when the frequency of actuation is ω_m. Using the delta function to evaluate the convolution integral, we get

$$f_m(t) \simeq \mathrm{Re}\{\tau_m^{\mathrm{mod}} \tilde{A}_m(t - D_m^{\mathrm{mod}}) e^{i(\omega_m t - \phi_m^{\mathrm{mod}})}\}, \quad (9)$$

where we have introduced the group delay $D_m^{\mathrm{mod}} \equiv \frac{d\phi}{d\omega}|_{\omega_m}$. The effective detuning $\delta f_{\mathrm{comp}}(t)$ of the cavity in response to the perturbation given in Eq. (5) is thus given by

$$\begin{aligned}\delta f_{\mathrm{comp}}(t) &= \delta f_{\mathrm{ext}}(t) + \sum_m f_m(t) \\ &= \delta f_{\mathrm{ext}}(t) + \sum_m \mathrm{Re}\{\tau_m^{\mathrm{mod}} \tilde{A}_m(t - D_m^{\mathrm{mod}}) e^{i(\omega_m t - \phi_m^{\mathrm{mod}})}\},\end{aligned} \quad (10)$$

where we have combined the tuner response at different frequencies and $\delta f_{\mathrm{ext}}(t)$ is the microphonics detuning coming from external vibrations. Now we can use this model to construct a suitable cost function which can be minimized by the algorithm.

The objective of microphonics compensation is to reduce the mean square detuning of the cavity:

$$C(t_n) \equiv \frac{1}{N} \sum_{i=n-N+1}^{n} [\delta f_{\mathrm{comp}}(t_i)]^2. \quad (11)$$

$C(t_n)$ is the cost function at time t_n which is taken to be the expectation value of the square of detuning, approximated by a running average. The method of gradient descent relies on the gradient vector being in the direction of steepest descent on the cost surface. In parameter space, the gradient represents the normal to the constant cost surface and can be estimated using the model developed in Eq. (10). Following standard LMS techniques [22], we use the current sample to approximate the cost function and hence use the stochastic gradient descent approach to the optimization problem. Taking $N = 1$, we calculate the partial derivatives of the cost function with respect to the optimization parameter $\tilde{A}_m$ which determines the actuator voltage:

$$\frac{\partial C}{\partial \tilde{A}_m} = \tau_m^{\mathrm{mod}} \delta f_{\mathrm{comp}}(t_n) e^{i(\omega_m t - \phi_m^{\mathrm{mod}})}, \quad (12)$$

where we have used Eq. (10) under the assumption that group delay D_m^{mod} is negligible with respect to the time scales with which $\tilde{A}_m(t)$ changes. The typical group delay introduced by the modified Saclay-I tuners used in the CBETA project is less than a millisecond far from resonant frequencies while the bandwidth of the vibration sources are typically less than 1 Hz. Each iteration of the stochastic gradient descent algorithm changes the control parameter a little in the direction opposite to the gradient.

$$\tilde{A}_m(t_{n+1}) = \tilde{A}_m(t_n) - \mu_m \delta f_{\mathrm{comp}}(t_n) e^{i(\omega_m t - \phi_m^{\mathrm{mod}})}, \quad (13)$$

where we have absorbed τ_m^{mod} into μ_m, which is the adaptation rate for $\tilde{A}_m$ in the algorithm. Equation (5) together with (13) form the active noise control (ANC) algorithm.

The ANC algorithm derived above is mathematically equivalent to applying a linear time invariant filter on the tuning error defined as $e(t) \equiv \delta f_0 - \delta f_{\mathrm{comp}}$ in order to generate the actuator signal $u_m(t)$, where we use $\delta f_0 = 0$ in the presence of no beam loading. To derive the equivalent filter transfer function, we start by assuming $\tilde{A}_m(0) = 0$, and write the update rule using the phasor notation,

$$\tilde{A}_m(t_{n+1}) = \sum_{k=0}^{n} [-\delta f_{\mathrm{comp}}(t_k)] e^{-i(\omega_m t_k - \phi_m^{\mathrm{mod}})}. \quad (14)$$

Combining this equation with the definition $u_m(t) \equiv \mathrm{Re}\{\tilde{A}_m(t) e^{i\omega_m t}\}$, we directly relate the actuator signal to the tuning error:

$$\begin{aligned}u_m(t_{n+1}) &= \mathrm{Re}\left\{\mu_m e^{i\omega_m t_{n+1}} \sum_{k=0}^{n} [-\delta f_{\mathrm{comp}}(t_k)] e^{-i(\omega_m t_k - \phi_m^{\mathrm{mod}})}\right\} \\ &= \mu_m \sum_{k=0}^{n} e(t_{n-k}) \cos[\omega_m (k+1)\Delta t + \phi_m^{\mathrm{mod}}],\end{aligned} \quad (15)$$

where Δt is the sample duration, and $e(t) = -\delta f_{\mathrm{comp}}(t)$. Equation (15) represents a discrete convolution of the input signal with a sinusoid and is an impulse response filter. The Z transform of the filter can be written as

$$\begin{aligned}H_m(z) &= \mu_m \sum_{k=0}^{\infty} z^{-k} \cos[\omega_m (k+1)\Delta t + \phi_m^{\mathrm{mod}}] \\ &= \mu_m \frac{\cos(\omega_m \Delta t + \phi_m^{\mathrm{mod}}) - z^{-1} \cos \phi_m^{\mathrm{mod}}}{1 - 2\cos(\omega_m \Delta t) z^{-1} + z^{-2}}.\end{aligned} \quad (16)$$

The frequency response is shown in Fig. 3.

The control filter shows a very narrow bandpass response rising to ∞ and a phase swing of 180° around the frequency ω_m. In the limit of $\omega \to \omega_m$, the filter response can be approximated by

$$H_m(e^{i\omega\Delta t}) \approx \frac{\mu_m e^{i(-\frac{\pi}{2} + \phi_m^{\mathrm{mod}} + \omega_m \Delta t)}}{2(\omega - \omega_m)\Delta t}. \quad (17)$$

μ_m serves as an overall scaling factor governing the span of frequencies within which the controller-tuner system has more than unity gain and μ_m can hence be used to adjust the

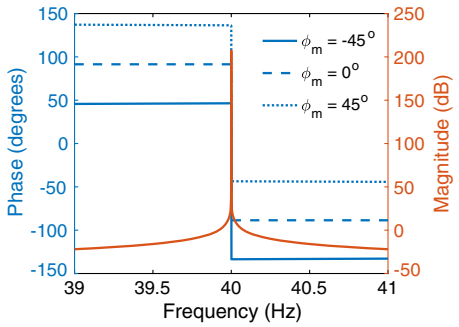

FIG. 3. Frequency response $H_m(e^{i\omega\Delta t})$ of the control filter described in Eq. (15) for one mode $f_m = 40$ Hz, $\mu_m = 10^{-4}$, $\Delta t = 0.1$ ms and three values of phase $\phi_m = -45°, 0°, 45°$. The value of ϕ_m primarily provides a constant offset to the phase response and can be used as a knob to stabilize the feedback control loop.

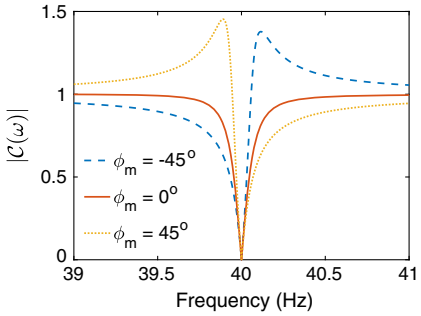

FIG. 4. Magnitude of closed loop transfer function in frequency domain with $f_m = 40$ Hz, $\mu_m = 10^{-4}$, $\Delta t = 0.1$ ms for different choices of ϕ_m when $\tau(\omega) = 1$. Regardless of the value of ϕ_m, microphonics at the frequency f_m is perfectly compensated.

bandwidth of the feedback loop around the microphonics frequency. In the neighborhood of ω_m, the phase swings from $\pi/2 + \phi_m + \omega_m\Delta t$ to $-\pi/2 + \phi_m + \omega_m\Delta t$ from left to right in a discrete jump.

B. Stability

The compensated detuning $\delta\tilde{f}_{\text{comp}}(\omega)$ is the net effect of the tuner $\delta\tilde{f}_m(\omega) \equiv \tau(\omega)u(\omega)$ and the external contribution $\delta\tilde{f}_{\text{ext}}(\omega)$. The tuner excitation $u(\omega) \equiv -H(\omega)\delta\tilde{f}_{\text{comp}}(\omega)$ is obtained as an output of the linear controller whose frequency response is given by $H(\omega)$. From these definitions we obtain the closed loop transfer function of the system which provides a linear relation between the external detuning $\delta\tilde{f}_{\text{ext}}(\omega)$ and the compensated detuning $\delta\tilde{f}_{\text{comp}}(\omega)$ in frequency space:

$$\mathcal{C}(\omega) \equiv \frac{\delta\tilde{f}_{\text{comp}}(\omega)}{\delta\tilde{f}_{\text{ext}}(\omega)} = \frac{1}{1 + \sum_m H_m(\omega)\tau(\omega)} = \prod_m \frac{1}{1 + H_m(\omega)\tau(\omega)}, \tag{18}$$

where the sum of all the filters $H(\omega) \equiv \sum_m H_m(\omega)$ acts as a comb with its frequency response amplitude remaining small except for the neighborhood of ω_m. This lets us write the transfer function as a product, since $|H_m(\omega)H_n(\omega)\tau^2(\omega)| \approx 0 \;\forall\; m \neq n$. In a theoretical situation, when all the microphonics detuning is generated by pure sine waves whose frequencies are exactly ω_m, the controller works perfectly to compensate for all microphonics. Figure 4 demonstrates this by showing that $|\mathcal{C}(\omega)|$ equals 0 at ω_m, where $\delta f_{\text{ext}}(\omega)$ only consists of a sine wave at exactly ω_m. However real microphonics signals have finite bandwidth spectral modes and the performance of feedback control is determined by the combined response of the controller and the tuner over all of frequency space. In the limit of the response of each filter being much greater near its passband than its nearest neighbors, we can approximate the complete tuner transfer function $\tau(\omega)$ with tuner transfer function models $\tau_m(\omega) \equiv \lim_{\omega\to\omega_m}\tau(\omega)$ at each compensation frequency ω_m:

$$\mathcal{C}(\omega) \sim \prod_m \frac{1}{1 + H_m(\omega)\tau_m(\omega)}. \tag{19}$$

Figure 4 shows the shape of one such isolated function and illustrates how adjusting ϕ_m can lead to an asymmetric response, attenuating vibrations on one side and amplifying the other. Further, the closed loop stability all of the individual contributions with index m can be a sufficient condition for the stability of the entire system.

In practice, we estimate the values of μ_m and ϕ_m^{mod} based on the measured tuner transfer function in order to configure the controller. If these guesses are close to the actual behavior of the tuner near ω_m, then the controller yields good performance and is stable. Approximating the *actual* tuner transfer function by $\lim_{\omega\to\omega_m}\tau(\omega) = \tau_m e^{-i\{\phi_m + D_m(\omega-\omega_m)\}}$, we can determine the range of values of μ_m and ϕ_m^{mod}, which leads to stable performance of the narrow band ANC algorithm.

We can analyze the stability of the feedback loop using the open loop transfer function $\mathcal{U}_m(\omega) \equiv H_m(\omega)\tau(\omega)$. The phase response ϕ_{OL} of $\mathcal{U}_m(\omega)$ around the frequency ω_m is given by

$$\phi_{\text{OL}} = \begin{cases} \frac{\pi}{2} + \phi_m^{\text{mod}} + \omega_m\Delta t - \phi_m - (\omega - \omega_m)D_m, & \text{for } \omega \leq \omega_m \\ -\frac{\pi}{2} + \phi_m^{\text{mod}} + \omega_m\Delta t - \phi_m - (\omega - \omega_m)D_m, & \text{for } \omega > \omega_m, \end{cases} \tag{20}$$

where ϕ_m^{mod} is the compensation parameter used in the control algorithm. The ANC response function [Eq. (16)] does not have any poles in the positive half of the complex plane. Using this information, the Nyquist stability criterion dictates that instability can only happen if $\mathcal{U}_m(\omega)$ encircles the point -1 in the complex plane. This occurs when $\mathcal{U}_m(\omega)$ crosses the negative real axis while $|\mathcal{U}_m(\omega)| \geq 1$. The band of frequencies within which instability may occur is given by

$$\omega_m - \frac{\mu_m \tau_m}{2\Delta t} < \omega < \omega_m + \frac{\mu_m \tau_m}{2\Delta t}. \tag{21}$$

The control loop is stable when we avoid positive feedback inside the above domain, i.e., $\phi_{\mathrm{OL}}(\omega_m - 0.5\mu_m\tau_m/\Delta t) < \pi$ and $\phi_{\mathrm{OL}}(\omega_m + 0.5\mu_m\tau_m/\Delta t) > -\pi$. This gives us a range of possible values for ϕ_m^{mod}:

$$\begin{aligned} -\frac{\pi}{2} + \frac{\mu_m \tau_m D_m}{2\Delta t} - \omega_m \Delta t + \phi_m < \phi_m^{\mathrm{mod}} \\ < \frac{\pi}{2} - \frac{\mu_m \tau_m D_m}{2\Delta t} - \omega_m \Delta t + \phi_m \end{aligned} \tag{22}$$

The center of the above range, $\phi_m^{\mathrm{center}} = \phi_m - \omega_m \Delta t$ compensates for the phase lag from the tuner at frequency ω_m and gives us the maximum margin on ϕ_m^{mod}. The span of acceptable values of ϕ_m^{mod} depends on not only the tuner behavior but also the adaptation rate μ_m. To ensure that the range given by Eq. (22) is not a null set, we put an upper bound on μ_m:

$$\mu_m < \frac{\pi \Delta t}{D_m \tau_m}. \tag{23}$$

These calculations assume that neighboring frequencies of the comb are far away so that their response amplitudes are much less than unity at the next frequency, i.e., $|\mathcal{U}_{m-1}(\omega_m)| = |\tau(\omega_m) H_{m-1}(\omega_m)| \ll 1$. This gives us a crude limit on the distance between nearest neighbors as

$$|\omega_m - \omega_{m-1}| \gg \frac{\mu_{m-1}\tau_m}{2\Delta t}, \tag{24}$$

hence constraining the spacing of the different frequencies we can compensate. Detailed calculations involving the complete tuner transfer function and the array of bandpass filters are required to fully analyze the stability of the control system.

The complete stability analysis of the ANC system involves assessing the open loop transfer function $\mathcal{U}_m(\omega)$ over all frequencies using a Bode plot. Figure 5 shows an example of using the compensation system on an unstiffened cavity used in the main linac of the CBETA project. We apply the algorithm on two frequencies 8 and 40 Hz illustrated by the notches in amplitude and expected phase swings of 180° at these frequencies. The open loop

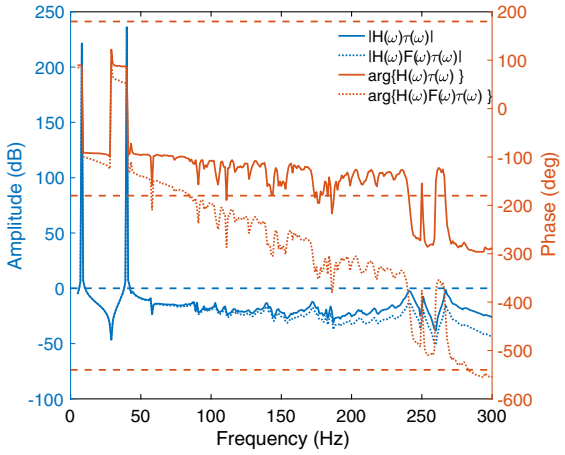

FIG. 5. Bode plot for the mechanical open loop transfer function $\mathcal{U}(\omega) \equiv H(\omega)\tau(\omega)$ of an unstiffened cavity inside the main linac used for the CBETA project, showing both the amplitude and phase in blue and orange respectively. The solid lines represent the effect of the active noise control algorithm applied to frequencies 8 and 40 Hz, while the dotted lines represent the effect of incorporating a low pass finite impulse response filter with frequency response $F(\omega)$ inside the controller. The blue dashed line represents unity gain (0 dB) and the orange dashed lines at $-540°, -180°$ and 180° represents the boundaries of stability in phase.

phase stays between the $-180°$ and 180° lines for gains above 0 dB showing that the system is stable near these frequencies. The phase margins, i.e., the distances from the $-180°$ line when the amplitude crosses unity gain (0 dB), are 80° and 90° at 8 and 40 Hz respectively as seen from the plot of $\phi_{\mathrm{OL}} = \arg\{H(\omega)\tau(\omega)\}$ in Fig. 5. However, the gain seems to be close to 0 dB near the tuner resonances at frequencies around 250 Hz, when ϕ_{OL} crosses the -180^o mark with a gain margin $\lesssim 2$ dB. This prompts the use of a low pass filter with frequency response $F(\omega)$ to attenuate the transfer function at these frequencies as shown by the dotted lines of Fig. 5. The analysis illustrates the effect of tuner resonances far from the compensation frequencies ω_m signalling the need for additional filtering to ensure stability of the system.

C. Performance on a single resonance

The performance of the controller in suppressing microphonics detuning depends on the vibrating components. Assuming that the microphonics is generated by resonant processes for example through thermoacoustic instabilities or through white noise excitations, the ensemble averaged power spectrum $\langle|\delta\tilde{f}_{\mathrm{ext}}(\omega)|^2\rangle_{\mathrm{E}}$ of mechanical eigenmodes is given by

$$\langle|\delta\tilde{f}_{\mathrm{ext}}(\omega)|^2\rangle_{\mathrm{E}} \equiv \sum_v \frac{\Gamma_v^2}{\{1 - (\frac{\omega}{\omega_v})^2\}^2 + (\frac{\omega}{Q_v\omega_v})^2}, \tag{25}$$

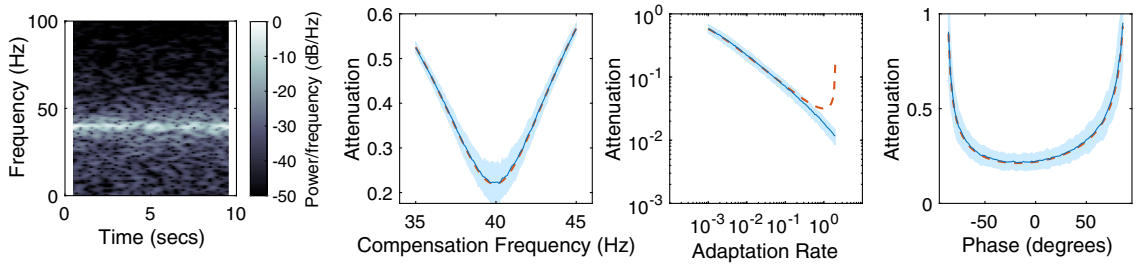

FIG. 6. Simulation results of using ANC with an ideal tuner. From the left, the first panel shows the spectrogram of simulated vibrations and the others show dependence of the attenuation $\sqrt{\langle \delta f_{\mathrm{comp}}^2 \rangle_t / \langle \delta f_{\mathrm{ext}}^2 \rangle_t}$ on frequency ω_m, adaptation rate μ_m and controller phase ϕ_m^{mod} respectively. The average of attenuation over an ensemble of 100 simulations is shown as the thin blue line and its 2σ confidence bounds are shaded light blue. The dashed red lines show the prediction from the model.

where ω_v, Q_v and Γ_v are the frequencies, quality factors and strengths of microphonics detuning. Using this prescription, we simulate the performance of the controller on vibrations generated by exciting a simple harmonic oscillator with frequency 40 Hz and quality factor 50 with Gaussian white noise from a random number generator with an arbitrary seed. The first panel of Fig. 6 shows the frequency content of detuning used to test the ANC controller. Assuming that the tuner transfer function, $|\tau(\omega)| = 1$ over all frequencies, we calculate the compensated detuning in each iteration as $\delta f_{\mathrm{comp}}(t_n) = \delta f_{\mathrm{ext}}(t_n) + u_{\mathrm{pz}}(t_{n-1})$. We simulate the mechanical performance of the controller-tuner system by iterating through Eqs. (13) and (5) to calculate the control signal $u_{\mathrm{pz}}(t_n)$ to the actuator, while the sampling and iteration process generates a group delay $D = 2\Delta t$. The performance of the system is calculated as $\sqrt{\langle \delta f_{\mathrm{comp}}^2 \rangle_t / \langle \delta f_{\mathrm{ext}}^2 \rangle_t}$ which represents attenuation of the microphonics detuning δf_{ext} excited by vibrations. To account for the randomness of the vibration signal, we perform the ensemble average of attenuation over 100 simulations using different random number seeds, each lasting for a duration of 10 seconds. We compare the results of the time domain simulations with the expected performance of the algorithm calculated semianalytically using the closed loop transfer function [Eq. (19)] along with the filter response in Eq. (16).

Figure 6 shows the simulated performance of the ANC algorithm under varying compensation parameters. The results show that the controller performs its best on average when $\omega_m = \omega_v$, with attenuation progressively getting worse as we go farther away from ω_v. The attenuation shows an asymmetric dependence on ϕ_m^{mod} about 0^o reaching a minimum at some nonzero value. Finally, μ_m represents the gain in the system and compensation is expected to get better with larger gain up to the limit given by Eq. (23) beyond which the system becomes unstable. The expected attenuation estimated from the semianalytical calculation clearly diverges at $\mu_m \gtrsim \pi/2$, however the results from the numerical simulations do not agree. In practice the maximum gain of the system will depend on the exact response of the tuner, especially the group delay. These simulations guide us on how to choose parameters of the ANC during operations.

D. Phase adaptation

The compensation performance of a controller with fixed parameters is dependent on variations in the response of the tuner and fluctuations of the microphonics spectrum. The tuner response may vary from day to day due to pressure variation in the helium bath while the vibration mechanism may also change frequency as a function of time. The controller as described in the previous section will not be able to adapt to such changes, which might limit performance in a dynamic environment. The simulation results in Fig. 6 suggest that attenuation is a monotonously decreasing function of gain μ_m, with the system becoming unstable beyond a threshold. An adaptive algorithm to optimize for the value of μ_m might tend to drive the system towards instability. However, the controller frequency ω_m and phase ϕ_m^{mod} have positions where attenuation is minimum within the range of values which satisfy the stability conditions. Consequently, adapting ω_m and ϕ_m^{mod} to a changing excitation could potentially make the algorithm more robust, while making it easier to operate in practice since it would optimize itself.

The optimization of the ANC system translates to finding the minimum of the mean square of detuning $\langle \delta f_{\mathrm{comp}}^2 \rangle$ with respect to the phases ϕ_m^{mod} and the frequencies ω_m. We can implement this optimization in the frequency domain using Parseval's theorem and Eq. (18) to establish a relation with $H_m(\omega)$:

$$\langle \delta f_{\mathrm{comp}}^2 \rangle_t \propto \int_{-\infty}^{\infty} |\delta \tilde{f}_{\mathrm{comp}}(\omega)|^2 \mathrm{d}\omega = \int_{-\infty}^{\infty} \left| \frac{\delta \tilde{f}_{\mathrm{ext}}(\omega)}{1 + \sum_m H_m(\omega)\tau(\omega)} \right|^2 \mathrm{d}\omega. \quad (26)$$

We can use this expression with any numerical optimizer to calculate the best values for the ANC parameters provided that the detuning spectrum $\tilde{f}_{\mathrm{ext}}(\omega)$ and the tuner transfer

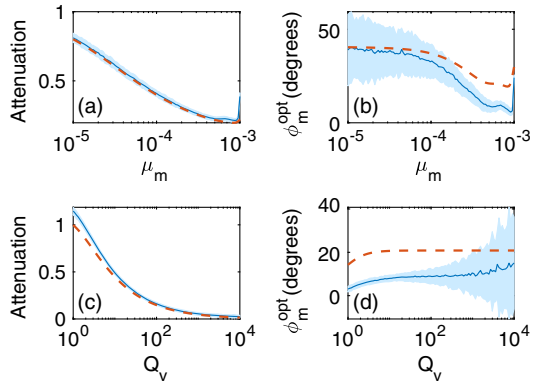

FIG. 7. Comparison of controller phase optimization for different gains and quality factors of vibration. (a) and (c) show the best attenuation reached while (b) and (d) show the optimum phase as functions of μ_m and Q_v respectively. Results from off-line optimization are shown as dashed lines while simulations of stochastic gradient descent are shown as the thin blue lines with 2σ confidence bounds shaded light blue.

function $\tau(\omega)$ are known. We simulate the performance of this approach by exciting vibrations at 40 Hz in δf_{ext} with varying quality factors Q_v and different μ_m in H_m. We use the measured $\tau(\omega)$ from unstiffened cavity 3 whose transfer function was shown in Fig. 1. Figure 7 shows the results from a simplex optimizer as dashed lines, with panels (b) and (d) showing the optimum values of phase ϕ_m^{opt} as a function of quality factor Q_v and adaptation rate μ_m respectively. Panels (a) and (c) show the minimum attenuation achieved by the optimizer.

In order to implement this optimization as a LMS scheme, we will need to adapt to changing characteristics of microphonics detuning in δf_{ext} and also measure tuner response $\tau(\omega)$ over the relevant frequencies at the same time. We derive an alternative algorithm which achieves this by solely adapting the controller phase ϕ_m^{mod} in order to minimize the cost function through gradient descent, and at the same time, make the controller more robust to changes in the tuner. The partial derivative of the cost function given in Eq. (11) with respect to ϕ_m^{mod} is given by

$$\frac{\partial C}{\partial \phi_m^{\text{mod}}} = 2\tau_m \delta f_{\text{comp}}(t_n) \text{Re}\{\tilde{A}_m(t_n) e^{i(\omega_m t_n - \phi_m(t_n) - \pi/2)}\}. \quad (27)$$

This gives us the update rule

$$\phi_m^{\text{mod}}(t_{n+1}) = \phi_m^{\text{mod}}(t_n) - \eta_m \delta f_{\text{comp}}(t_n) \times \text{Re}\{\tilde{A}_m(t_n) e^{i(\omega_m t_n - \phi_m^{\text{mod}}(t_n) - \pi/2)}\}, \quad (28)$$

where η_m is the adaptation rate for ϕ_m^{mod}. Figure 7 also shows the results from simulations of this algorithm with microphonics at frequency $f_v = 40$ Hz, with a tuner response modeled on the same measured $\tau(\omega)$ for MLC cavity 3. We initialized the simulations with the known microphonics frequency $f_m = f_v = 40$ Hz, an initial guess for the tuner phase $\phi_m^{\text{mod}} = 0$ and phase adaptation rate $\eta_m = -0.0001$. We set the controller gain to $\mu_m = 0.0006$ for the simulations with varying Q_v, and set the quality factor of vibration source to $Q_v = 50$ for simulations with different μ_m. The thin blue lines representing the ensemble average over 80 simulations clearly show the LMS adapted phase deviates from the simplex optimization outlined in the previous paragraph. This deviation arises from the approximate model [Eq. (10)] of compensated detuning which we used to construct the partial derivative as we have neglected group delay and higher order terms in Eq. (7). However, the attenuation obtained from gradient descent closely matches the ideal result, thus demonstrating the efficacy of this method.

IV. RESULTS

The Cornell-BNL ERL test accelerator (CBETA) [7,23,24] project will be the first high-current multiturn ERL employing SRF Linacs. It uses two SRF cryomodules, one for the injection system and the other used to execute energy recovery. The injector cryomodule [25,26] consists of five two-cell SRF cavities [27] and is configured to provide 6 MeV of energy gain to the electron beam for injection into the CBETA loop and is operated with a low external quality factor due to high beam loading. The main linac [11,28] on the other hand incorporates six seven-cell SRF cavities [29] with a design energy gain of 36 MeV and will be used to execute energy recovery. Operated at $Q_L \approx 6 \times 10^7$ with solid state amplifiers, the peak detuning which can be tolerated by the main linac cavities is limited to 54 Hz with a 5 kW rf source, consequently microphonics detuning presents a significant operational bottleneck and needs to be mitigated.

A. Passive suppression

The initial microphonics measurements of the main linac cavities showed strong vibrations at frequencies 8, 41 and 82 Hz as illustrated in the plots of rms detuning in Fig. 8. Apart from steady vibrations at these frequencies, sudden events resulting in large peak detuning of over 100 Hz were seen in the unstiffened cavities 3 and 5 as evident from the histograms. Vibrations can mechanically couple into the cavities from sources both inside and outside the cryomodule. In an attempt to find them, we cross-correlated the microphonics detuning signal with vibration signatures from various machinery. We started with the rotary and turbomolecular pumps maintaining the insulation vacuum in the cryomodule, looking at the effect of power cycling them for brief periods and eventually calculating the cross-correlation functions. Though the rotary pump did not have any effect, the turbomolecular pump does induce weak vibrations around 820 Hz, consistent with a rotation speed of 50000 rpm. There are large variable frequency induction

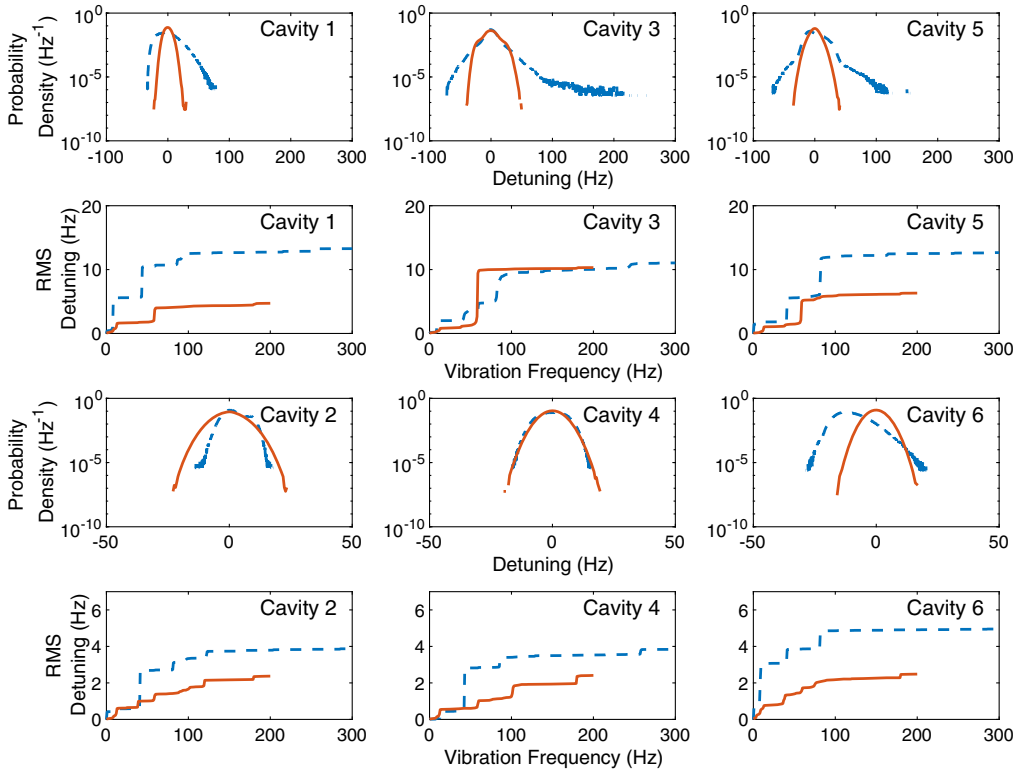

FIG. 8. Microphonics measurements on all cavities of the main linac before and after the modifications of the cryogenic system. The dashed lines represent data from the default configuration for cavities 2, 3, 5 and 6; while the data for cavities 1 and 4 were taken after making the Joule-Thomson (JT) and precool valves static. The solid lines indicate data after the JT and precool valves were made static and the 5 K adjust valve was fitted with sleeves.

motor water pumps on the experimental floor in the vicinity of the cryomodule, these were also shown to be of no effect to the microphonics detuning. Further we also measured vibrations from the large room temperature vacuum pumps controlling the vapor pressure of helium inside the cryomodule, showing that these too do not contribute to peak detuning of the cavities directly. Besides direct mechanical coupling of vibrations through the cavity supports, pressure fluctuations in the liquid helium surrounding the cavity also give rise to microphonics detuning. Table I shows a summary of the different vibration sources and their relative contribution to the total rms detuning in the main linac cavities. In the original configuration, the pressure variations in liquid helium accounted for most of the microphonics in the main linac cavities.

The cryogenic system of the main linac cryomodule is a modified version of the TESLA design [30]. Separate vessels house the six cavities and are supplied with liquid helium through chimneys by the 2K-2 phase pipe and through the precool line connected to the bottom of the vessels. The pressure exerted by liquid helium on the cavity walls influences the resonant frequency of the cavities and

TABLE I. Contribution from various microphonics sources, listed as percent of total mean square microphonics detuning. Thermoacoustic oscillations from the 5 K adjust valve are responsible for vibrations at 41 and 82 Hz, forming the major source of microphonics in the original configuration measured in 2017. In contrast, vibrations coupled in through the new waveguides installed in 2018 are the major contributor to detuning in unstiffened cavities after valve modification.

	Cavity 1		Cavity 2		Cavity 3		Cavity 4		Cavity 5		Cavity 6	
Source	2017	2018	2017	2018	2017	2018	2017	2018	2017	2018	2017	2018
Low frequency	0.1	0.1	1.2	0	0	0	0	0	1.3	0	2.2	0
Gas flow 8 Hz	17	1.7	0.8	0.1	2.9	0.1	0	0.1	0.2	0.1	32.4	1.9
Valve 41 Hz	42.1	0.4	44.3	0.1	5.3	0.1	39.4	0.1	16.8	0.6	20.8	0.7
Waveguide 59 Hz	2.4	46.3	0.6	3.4	7.5	78.5	0.7	4.4	0.4	46.9	0.3	7.2
Valve 82 Hz	11.1	2.9	20	1.2	43.7	0.8	16.8	0.7	66	6.9	34.1	4.5
Miscellaneous	27.4	48.7	33.1	95	40.5	20.5	43.1	94.7	15.3	45.5	10.2	85.6

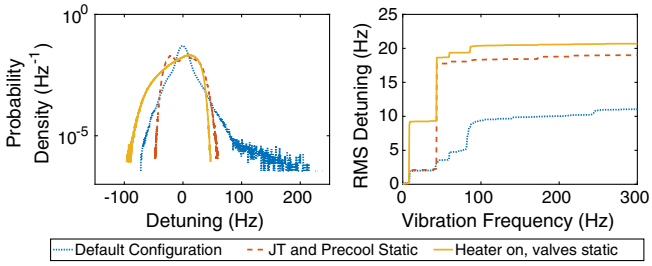

FIG. 9. Influence of valve actuation on microphonics detuning of cavity 3 (unstiffened) showing the detuning histogram on the left panel and the rms detuning on the right from measurements of duration 800 seconds.

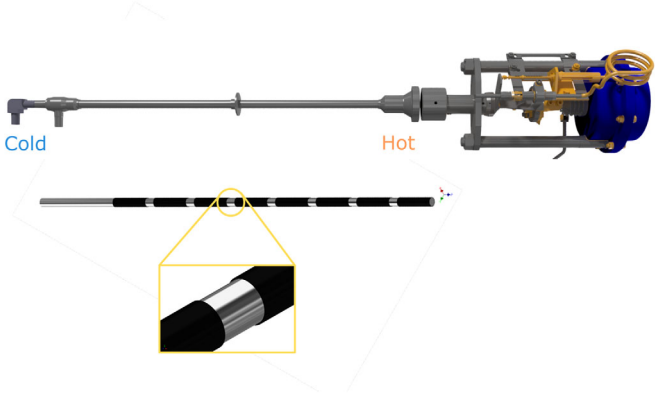

FIG. 10. Cryogenic needle valve used to regulate helium flow in the cryomodule and the electro-pneumatically actuated valve stem showing attached plastic sleeves filling the space between the stem and the inner surface of the stalk.

needs to be regulated. Slow trends in this pressure give rise to very low frequency microphonics detuning ($\lesssim$1 Hz) and tight pressure regulation requires the interplay of two control mechanisms. A Joule-Thomson (JT) valve maintains the liquid level in the 2K—2 phase pipe and an external pump maintains the vapor pressure near 12.5 Torr corresponding to 1.8 K. Two separate proportional integral feedback loops actuate the JT valve and control the pump to maintain the liquid level and vapor pressure at their set points respectively. The system also opens the precool valve when the liquid level goes below a threshold. Consequently, transients or instabilities in any of these components may give rise to vibrations in the cryomodule.

Measurements of microphonics detuning and various cryogenic control parameters showed that movement of the JT and movement of the precool valve both coincided with the large peak detuning events. The occasional actuation of the precool valve in response to the helium liquid level going below a threshold correlated with spikes in a signal from a piezoelectric sensor. However the occurrence of peak detuning is more frequent, consequently we made both the precool and the JT valves static and the results of this test are shown in Fig. 9. In the default configuration, the microphonics histogram shows large peak events which are $\gtrsim$200 Hz,[2] while the peak microphonics detuning becomes ~50 Hz with both valves static verifying the proposed mechanism. However, this configuration does not allow us to have active control on the liquid helium level and if the boil off generated due to the thermal load from the cavities does not equal the rate of in-flow from the supply line, then the liquid level in the 2K—2 phase pipe would steadily run away. To avoid this, a heater attached to the 2K—2 phase pipe is put on a control loop to provide a minimum dynamic thermal load to substitute for when the cavities are not generating enough heat and thus boiling off suitable amounts of helium while stabilizing the liquid level. This results in stable operation while limiting the peak detuning to ~100 Hz a definite improvement from the original configuration. Despite the additional detuning introduced due to the operation of the heater, this is still better than controlling the helium level using the valves.

Peak detuning was greatly improved when the valves were made static, however we observed a strong enhancement of the steady state oscillations at 41 Hz which do not contribute much to the peak detuning but increase the rms by a factor of 2. The liquid helium level control using the heater enhances the narrow band 8 Hz vibration line. This points to gas flow in the helium gas return pipe as a possible source for the generation of the 8 Hz vibrations. Previous operations data further corroborated this fact by showing that the vibration amplitude at 8 Hz is an increasing function of the vapor flow through the helium gas return pipe possibly exciting a mechanical eigenmode of the structure. Pending further investigation into the source, the active compensation system has been successful in attenuating these vibrations.

Accelerometer measurements of vibration on the 5 K adjust cryogenic valve stalk yielded significant cross-correlation with the microphonics detuning measurement at 41 and 82 Hz. Figure 10 is a schematic of the valve showing the cold region near the valve orifice which comes in contact with cold helium and the warm region which extends outside the cold mass of the cryomodule and is at room temperature. Delayed heat transfer between the hot and the cold regions through convection of the helium gas and conduction through the valve stalk leads to thermoacoustic oscillations [31] and the resulting pressure waves resonate inside the closed space between the valve stem and the valve stalk. This mechanism of vibrations was first observed in the LCLS-II cryomodules while testing at Fermilab [32]. Following discussions with the Fermilab team, we inserted sleeves made of a cryogenic compatible PEEK plastic material on the stem to restrict the gas flow and suppress vibrations [33].

[2]A slight offset in the phase calibration of the field probe signal might have led to this uncharacteristically large value of peak detuning. However all data shown in Fig. 9 were taken with the same calibration settings and so this is a valid verification of the valve actuation effect.

TABLE II. Microphonics measurements before and after cryogenic system modifications for both stiffened and unstiffened cavities. The third column shows the pressure to detuning coefficient df/dp. Root mean square detuning is calculated from the detuning histograms except for the values in brackets which are obtained from the spectrum plots and are band limited to 200 Hz.

		df/dp	Peak detuning (Hz)			rms detuning (Hz)		
Cavity	Stiffened	(Hz/Torr)	Original	JT and precool static	5 K adjust modified	Original	JT and precool static	5 K adjust modified
1	No	38	N/A	78	30	N/A	13.6	5.0 (4.7)
2	Yes	15	18	N/A	25	4.4	N/A	4.6 (2.4)
3	No	46	280[1]	100	50	11.2	20.8	10.7 (10.3)
4	Yes	17	N/A	17	20	N/A	4.4	3.7 (2.4)
5	No	33	163[1]	N/A	41	12.7	N/A	6.9 (6.3)
6	Yes	19	30	N/A	18	5.0	N/A	3.2 (2.5)

Table II shows a summary of the microphonics measurements on all cavities in different configurations of the cryogenic system. The peak detuning on all unstiffened cavities (Fig. 8) showed a significant reduction after the 5 K adjust valve was modified. Table I also demonstrates a significant reduction in the fractional contribution to the net mean square detuning from this instability at 41 and 82 Hz. However, we measured a new vibration line at 59 Hz which was not seen during our previous tests. The results from cross-correlation measurements of the microphonics detuning and accelerometer signals indicate that 59 Hz vibrations from an external source are being mechanically coupled into the cryomodule through the newly installed waveguides. The new source significantly contributes to mean square detuning on all the unstiffened cavities as shown in Table I. Cavity 3 is affected the most with the highest peak detuning (∼50 Hz) among all others and this was an excellent candidate for testing the active compensation system.

Stiffened cavities did not show a significant reduction in peak microphonics detuning, with an increase being shown by cavities 2 and 4 even when the rms diminished for cavity 4. Figure 8 shows results from microphonics measurements on these cavities. The histogram of detuning for cavity 2 and cavity 4 shows a flat top, indicating deviations from Gaussian white noise. The spectrum plot shows substantial vibration energy localized around 41 Hz and the 82 Hz corroborating this observation and the thermoacoustic oscillations are indeed the reason as discussed earlier. The spectrum plots further indicate a reduction of the energy after valve modification in the same frequency bands, along with a net decrease in rms detuning up to a vibration frequency of 200 Hz which is the limit of the dataset. However, the width of the histograms also related to the rms seems unchanged for cavity 4 and shows an increase in cavity 2 after valve modification seemingly contradicting the frequency domain observations. This apparent disagreement of the rms detuning obtained from the histogram and the spectrum plots are listed in Table II. While the estimates agree for unstiffened cavities, there is a significant difference for the stiffened cavities. The missing vibration energy could be accounted for by the excitation of high frequencies ($\gtrsim$200 Hz), possibly the mechanical eigenmodes of the cavity along with measurement noise. Unfortunately the raw signals were not recorded during this experiment rendering us unable to analyze this in more detail.

B. Active compensation

Passive measures of mitigating the vibration sources is the preferred method of reducing microphonics detuning. However active control is also necessary to temporarily restore operating gradient until the source is mitigated and to improve the margin of rf power consumption in the presence of existing microphonics detuning. We implemented the narrow band ANC algorithm in the Cornell digital low level rf control system [34,35] for this purpose. Figure 11 presents a simplified diagram of the rf system showing the relevant signal paths. We mix the rf signals from the cavity with an internal frequency reference to generate a baseband signal at 12.5 MHz. The field control loop runs at this frequency in a field programmable gate array (FPGA) which measures the amplitudes and phases of the field and the forward power, while the difference of the phases is used to determine the net microphonics detuning δf_{comp}. The processed detuning and field data are then transferred to a digital signal processor (DSP) which we use to execute resonance control. Besides LFD compensation and proportional integral control on low frequency microphonics, the DSP also incorporates the modified narrow band ANC algorithm we have proposed in this paper.

The implemented ANC algorithm requires prior knowledge of the frequency content of external vibrations but does not require any measurement of the tuner transfer function at the frequencies of interest. We first measure the spectrum of microphonics detuning and determine which frequencies we want to compensate. The algorithm is then applied separately on each of these known excitations at ω_m. It requires two additional parameters, the gain μ_m and phase adaptation rate η_m as described in Eqs. (13) and (28)

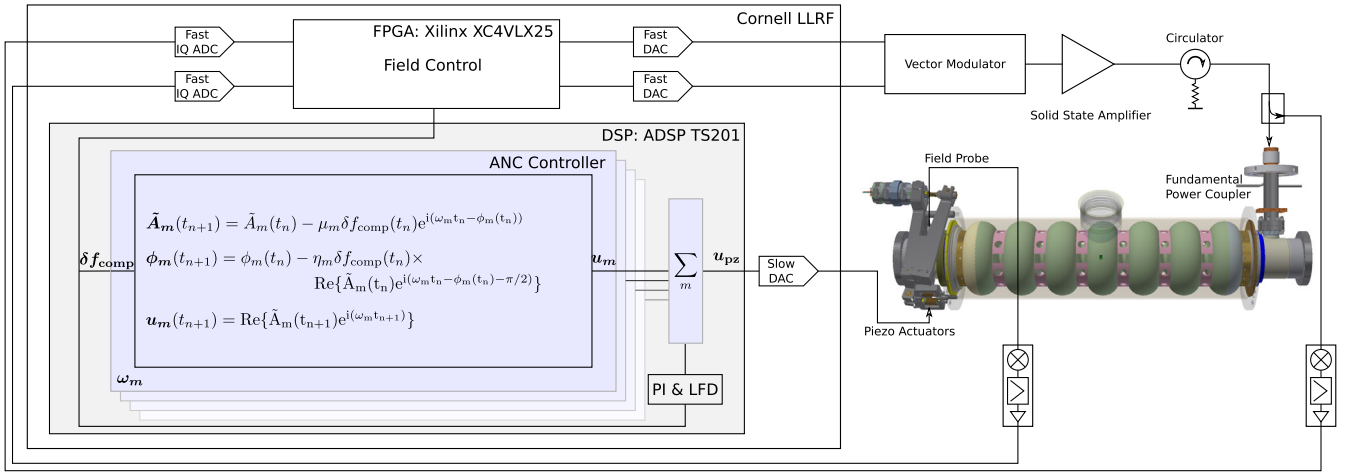

FIG. 11. Simplified diagram of the setup used during routine linac operations for CBETA. The Cornell low level radio frequency control system incorporates a FPGA responsible for field control and a digital signal processor (ADSP TS201) for executing comparatively slow tasks. The modified ANC algorithm [Eqs. (13), (28) and (5)] is executed inside the DSP for each microphonic spectral line at ω_m. The output of all the individual controllers u_m are summed and sent to the piezoelectric actuator. The diagram also shows proportional-integral control for low frequency microphonics along with a Lorentz force detuning compensation system.

respectively for each of these excitations. To determine an optimum setting, we start with small numbers for μ_m and η_m until we start observing some effects on the net microphonics detuning, increasing μ_m until the feedback loop becomes unstable. At the same time, we minimize the peak detuning by optimizing the value of ω_m which strongly determines the performance. We set μ_m to half of the maximum stable value to give us a suitable gain margin, and observe the controller phase ϕ_m as a function of time. We set η_m so that the phase settles to the optimum value on average within a few minutes at the same time showing a noise level within $\pm 10°$. This process is repeated for each frequency we want to compensate, while the overall performance of resonance control depends on the quality factors of vibrations as illustrated in Fig. 7.

We have used the ANC algorithm during various stages of rf commissioning to attenuate microphonics and the results from unstiffened cavities of the main linac are shown in Fig. 12. Before we modified the 5 K adjust valve, compensation was applied to 41 and 8 Hz on unstiffened cavities 1 and 3. The algorithm was successful in attenuating 41 Hz in both cavities 1 and 3 but was not effective on 8 Hz vibrations in cavity 3 as illustrated by the spectrum plots probably because the compensation frequency was not set precisely. These narrow band vibrations were a major contribution to microphonics detuning and their decrease also reduced the peak detuning. After we modified the 5 K adjust valve, we found the major source of microphonics detuning to be at 59 Hz. The ANC algorithm was successful in suppressing these vibrations in cavity 3. The attenuation of spectral lines are further validated by the rms detuning as listed in Table III. The success of the algorithm indicates that those vibration lines were not in the vicinity of mechanical eigenmodes of the tuner-cavity

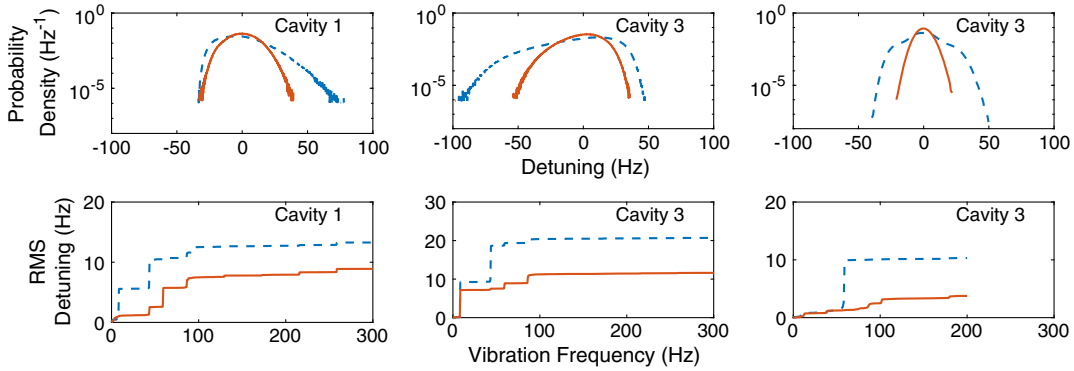

FIG. 12. Effect of active microphonics compensation on two unstiffened cavities of the main linac. The dashed lines represent data without active suppression while the bold lines show the performance with ANC turned on. The first two sets of data were taken before valve modification while the last dataset was taken after.

TABLE III. Results of using the active noise control system on various cavities during different stages of commissioning.

Run description	Peak detuning (Hz)		rms detuning (Hz)	
	ANC Off	ANC On	ANC Off	ANC On
Cavity 1 with JT and precool static	78	45	13.6	9.1
Cavity 3 with JT and precool static	100	57	20.8	11.7
Cavity 3 with JT and precool static and 5 K adjust valve modified	50	22	10.7	4.6
Cavity 4 with JT and precool static	17	19	4.4	2.4
Cavity 6 in original configuration	30	15	6.4	3.4

system which would have limited the effectiveness of the system as explained in Sec. III.

The results of using the system on stiffened cavities is shown in Fig. 13. The algorithm was applied to cavities 4 and 6 for the frequencies 8 and 41 Hz with additional attenuation of 82 Hz on cavity 6. While the ANC successfully reduced peak detuning from 30 to 15 Hz in cavity 6, the measurements on cavity 4 indicate no reduction of peak detuning even though the rms detuning is attenuated as seen from both the histogram and the spectrum plot. To understand which frequencies actually contribute to peak detuning, we Fourier transform the raw signal and zero all components beyond a certain vibration frequency and then find the peak detuning of the inverse transformed signal. Figure 14 shows the cumulative peak detuning as a function of the vibration frequency threshold. When the ANC is off, 41 and 82 Hz contribute most to the peak detuning as indicated by the large steps when we include these frequencies in the peak calculation. When we turn on compensation, the contribution from both these frequencies are reduced but a new mode at 102 Hz appears which accounts for almost half of the peak detuning but appears as a shallow step in the spectrum plot, illustrating its transient nature. These additional spectral lines generated by the ANC controller point to transients possibly

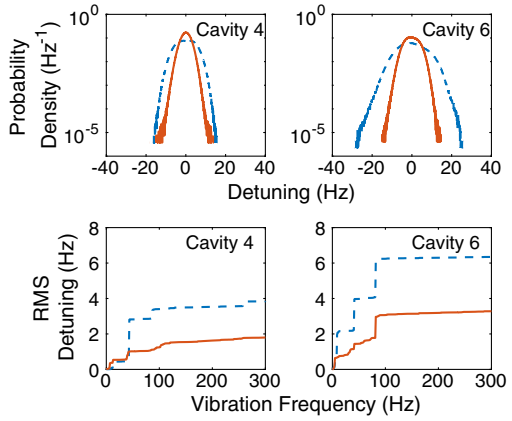

FIG. 13. Effect of active microphonics compensation on two stiffened cavities of the main linac. The dashed lines represent data without active suppression while the bold lines show the performance with ANC turned on.

generated by the nonlinear phase adaptation process. Nevertheless, the ANC algorithm is well suited for compensating narrow band vibrations in both stiffened and unstiffened cavities as evidenced from the performance listed in Table III.

The stability and robustness of the algorithm is demonstrated by comparatively long periods of stable operation with the same settings on different days. The observations shown in Table III are taken from datasets of at least 800 seconds measured for cavities inside a cryomodule connected to a production level cryogenic system unlike previous work primarily focused on test facilities. We achieved stable operations of over a few hours without spontaneous trips on all cavities with the ANC system active. We also successfully used it on cavity 3 during beam operations for the CBETA fractional arc test which helped us achieve an energy gain of 8 MeV using a forward power below 5 kW which would not be possible without it. Once the settings were determined using the procedure explained earlier, resonance control was turn key with no tweaking required on subsequent days of operation which highlights the robustness of the system.

Lorentz force detuning (LFD) and mechanical coupling between different cavities in the cryomodule can be further sources of detuning which affect the operation of a resonance control system. The field dependence of LFD leads to decrease in the resonant frequency when the cavity

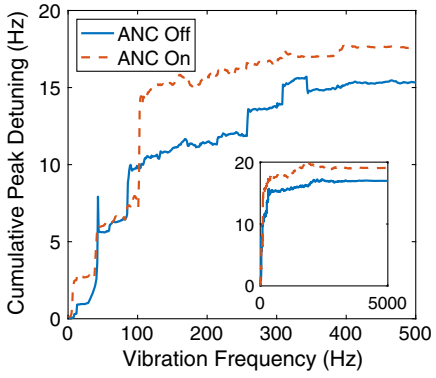

FIG. 14. Cumulative peak detuning as a function of frequency for cavity 4 before valve modification showing the effect of active noise control system.

field is ramped up. Large microphonics events generating a sudden increase in the resonance frequency of the cavity can lead to reduction in fields, LFD can in turn detune the cavity further in the positive direction amplifying the effect of the microphonics. Such an instability will lead to a catastrophic fall in cavity field and subsequent beam loss in an accelerator. However, in high Q machines the filling time of narrow bandwidth cavities can be sufficiently large, of the order of tens of milliseconds, slowing down the field decrease. This along with the presence of a high gain feedback loop on the field can be enough to avoid such an instability from developing. In all our operations until now, we have not used any feed-forward control of detuning and simple integral control of detuning has been enough to compensate for LFD when the field is ramped slowly. Further, the resonance control system of neighboring cavities did not interact with each other during the course of normal operation since we have bellows mechanically isolating the cavities. This eliminates the need to account for such effects. The resonance control system described in this paper is thus a stable way of reducing peak detuning when mitigation of vibration sources is not an option.

V. CONCLUSION

The operation of SRF cavities with high Q_L using solid state amplifiers of limited power present a significant constraint on the peak microphonics detuning which we can tolerate in order to maintain a stable field. As a result, mitigation of vibration sources has become important for operations for a growing number of particle accelerators. Apart from passive measures, most cryomodules also incorporate fast tuners based on piezoelectric actuators which can be used for active resonance control such as in LCLS-II and XFEL. Assuming that the mechanics is adequately described by linear partial differential equations, we can model the tuner's response as a slowly changing linear time invariant system. This lets us encode the dynamics of the tuner in a transfer function $\tau(\omega)$, which expresses the amplitude and phase response of the cavity resonance frequency to sinusoidal excitations applied to the actuator at different frequencies. Measurements from seven-cell SRF cavities used in the main linac of the CBETA project indicate that the bandwidth of an active control system must be limited to below microphonics frequencies of 200 Hz beyond which mechanical eigenmodes dominate the dynamics. The transfer function data is used in the design of the active microphonics control system.

We derived the narrow band active noise control (ANC) algorithm starting from the assumption that microphonics detuning can be decomposed into a finite sum of sine waves. A sine wave of the same frequency applied to the actuator at the correct amplitude and phase should perfectly compensate for the vibrations. Using stochastic gradient descent, we derived an update relation which slowly changes phasors with components I_m and Q_m depending on the net microphonics detuning. These in turn modulate carrier signals at the microphonics frequencies ω_m applied to the actuator thus completing the ANC feedback controller. We further derived the frequency response of the ANC algorithm and established constraints on the adaptation rates μ_m and the controller phases ϕ_m to operate in the stable region, giving one concrete example from CBETA. Finally we propose a modification which automatically minimizes the mean square of compensated detuning by adapting the value of the controller phase in response to changing tuner responses or changing vibration excitations. Using numerical simulations, we demonstrated the effectiveness of the modified ANC algorithm before it was implemented on the main linac used in CBETA.

We applied various mitigation techniques on the main linac cryomodule of the CBETA project to reduce microphonics detuning. Passive measures included several modifications to the cryogenic system to damp thermoacoustic oscillations and transients related to helium flow and we achieved a reduction of peak detuning by at least a factor of 2. We further demonstrate the use of the active control system to achieve a stable reduction of microphonics typically by a factor of 2 without the need of detailed measurement of the transfer function. Future work will involve finding the remaining sources of vibrations and eliminating them, incorporating automatic frequency tracking in the ANC algorithm in order to make it more robust, and devising an algorithm to automatically configure the ANC on multiple frequencies during operation. In addition, we also plan to measure energy and time of arrival jitter in the beam and correlate these measurements with microphonics detuning.

ACKNOWLEDGMENTS

We would like to thank Vadim Veshcherevich and Roger Kaplan for extensive help in setting up the rf systems, Eric Smith, Dan Sabol and Colby Shore for setting up the cryogenic systems including procuring the plastic sleeves and modifying the valve stem, and Adam Bartnik and Colwyn Gulliford for helping with operations. We are grateful to Warren Schappert and Ben Hansen for sharing the experience of commissioning the LCLS-II cryomodules at Fermilab which prompted us to look for thermoacoustic oscillations in our cryogenic valves. We are indebted to Claudio Rivetta and Douglas MacMartin for providing insight on theoretical aspects of our controller. This work was supported by the New York State Energy Research and Development Authority. CLASSE facilities are operated with major support from the National Science Foundation.

[1] H. S. Padamsee, Superconducting radio-frequency cavities, Annu. Rev. Nucl. Part. Sci. **64**, 175 (2014).

[2] T. Mastorides, C. Rivetta, J. D. Fox, D. Van Winkle, and P. Baudrenghien, Rf system models for the CERN large hadron collider with application to longitudinal dynamics, Phys. Rev. ST Accel. Beams **13**, 102801 (2010).

[3] S. Belomestnykh and H. Padamsee, Performance of the CESR superconducting rf system and future plans, *SRF Workshop, 2001*.

[4] J. Rose, W. Gash, B. Holub, Y. Kawashima, H. Ma, N. Towne, and M. Yeddulla, Nsls-ii rf systems, in *Proceedings of the 24th Particle Accelerator Conference, PAC-2011, New York, 2011* (IEEE, New York, 2011), FROBS4.

[5] L. Doolittle, G. Huang, A. Ratti, C. Serrano, R. Bachimanchi, C. Hovater, S. Babel, B. Hong, D. Van Winkle, B. Chase, E. Cullerton, and P. Varghes, The LCLS-II LLRF system, in *Proceedings of IPAC, 2015* (JACoW, Geneva, Switzerland, 2015), MOPWI021.

[6] J. Branlard, V. Ayvazyan, L. Butkowski, H. Schlarb, J. Sekutowicz, W. Cichalewski, A. Piotrowski, K. Przygoda, W. Jamuzna, and J Szewinski, Llrf system design and performance for XFEL cryomodules continuous wave operation, *SRF Workshop, 2013*, THP086.

[7] G. H. Hoffstaetter *et al.*, CBETA design report, Cornell-BNL ERL test accelerator, arXiv:1706.04245.

[8] M. Abo-Bakr *et al.*, Status report of the Berlin energy recovery linac project BERLinPro, in *Proceedings of the 9th International Particle Accelerator Conference (IPAC'18), Vancouver, BC, Canada, 2018* (JACoW Publishing, Geneva, Switzerland, 2018), p. 9, THPMF034.

[9] M. Liepe and S. Belomestnykh, Rf parameter and field stability requirements for the Cornell ERL prototype, in *Proceedings of the 2003 Particle Accelerator Conference, Portland, OR* (IEEE, New York, 2003), Vol. C030512, p. 1329.

[10] S. Posen and M. Liepe, Mechanical optimization of superconducting cavities in continuous wave operation, Phys. Rev. ST Accel. Beams **15**, 022002 (2012).

[11] R. Eichhorn *et al.*, Cornell's main linac cryomodule for the energy recovery linac project, in *Proceedings of the 5th International Particle Accelerator Conference (IPAC 2014), Dresden, Germany, 2014* (JACoW Publishing, Geneva, Switzerland, 2014), Number 5, WEPRI061.

[12] S. Posen and M. Liepe, Measurement of the mechanical properties of superconducting cavities during operation, in *Proceedings of the 3rd International Particle Accelerator Conference, New Orleans, LA, 2012* (IEEE, Piscataway, NJ, 2012), Vol. C1205201, pp. 2399–2401.

[13] Y. Pischalnikov, B. Hartman, J. Holzbauer, W. Schappert, S. Smith, and J.-C. Yun, Reliability of the LCLS II SRF cavity tuner, in *Proceedings of the 17th International Conference on rf Superconductivity (SRF2015), Whistler, Canada, 2015* (JACoW, Geneva, Switzerland, 2015), THPB065.

[14] W. Cichalewski, J. Branlard, A. Napieralski, and C. Schmidt, European XFEL cavities piezoelectric tuners control range optimization, in *Proceedings of the 15th International Conference on Accelerator and Large Experimental Physics Control Systems (ICALEPCS 2015), Melbourne, Australia, 2015* (JACoW, Geneva, Switzerland, 2015), MOPGF079.

[15] S. J. Elliott, M. Ghandchi Tehrani, and R. S. Langley, Nonlinear damping and quasilinear modeling, Phil. Trans. R. Soc. A **373**, 20140402 (2015).

[16] Z. Conway and M. Liepe, Fast piezoelectric actuator control of microphonics in the cw Cornell ERL injector cryomodule, in *Proceedings of the 23rd Particle Accelerator Conference, Vancouver, Canada, 2009* (IEEE, Piscataway, NJ, 2009), TU5PFP043.

[17] N. Banerjee *et al.*, Microphonics studies of the CBETA linac cryomodules, in *Proceedings of the International Particle Accelerator Conference (IPAC'17), Copenhagen, Denmark, 2017* (JACoW, Geneva, Switzerland, 2017), Number 8, pp. 1138–1141, https://doi.org/10.18429/JACoW-IPAC2017-MOPVA122.

[18] A. Neumann, W. Anders, O. Kugeler, and J. Knobloch, Analysis and active compensation of microphonics in continuous wave narrow-bandwidth superconducting cavities, Phys. Rev. ST Accel. Beams **13**, 082001 (2010).

[19] J. Holzbauer, B. Chase, L. Doolittle, J. Einstein-Curtis, Y. Pischalnikov, W. Schappert, and C. Serrano, Active microphonics compensation for LCLS-II, in *Proceedings of the 9th International Particle Accelerator Conference (IPAC 2018), Vancouver, BC, Canada, 2018* (JACoW, Geneva, Switzerland, 2015), WEPML007.

[20] T. H. Kandil, H. K. Khalil, J. Vincent, T. L. Grimm, W. Hartung, J. Popielarski, R. C. York, and S. Seshagiri, Adaptive feedforward cancellation of sinusoidal disturbances in superconducting rf cavities, Nucl. Instrum. Methods Phys. Res., Sect. A **550**, 514 (2005).

[21] R. Rybaniec, K. Przygoda, W. Cichalewski, V. Ayvazyan, J. Branlard, L. Butkowski, S. Pfeiffer, C. Schmidt, H. Schlarb, and J. Sekutowicz, FPGA-based rf and piezocontrollers for SRF cavities in cw mode, IEEE Trans. Nucl. Sci. **64**, 1382 (2017).

[22] S. M. Kuo and D. R. Morgan, Active noise control: A tutorial review, Proc. IEEE **87**, 943 (1999).

[23] G. Hoffstaetter *et al.*, CBETA: The Cornell/BNL 4-turn ERL with FFAG return arcs for eRHIC prototyping, in *Proceedings of the 28th International Linear Accelerator Conference (LINAC16), East Lansing, Michigan, 2016* (JACoW, Geneva, Switzerland, 2015), TUOP02.

[24] D. Trbojevic *et al.*, CBETA–Cornell University Brookhaven National Laboratory electron energy recovery test accelerator, in *Proceedings of the 8th International Particle Accelerator Conference (IPAC 2017), Copenhagen, Denmark, 2017* (JACoW, Geneva, Switzerland, 2015), TUOCB3.

[25] M. Liepe, G. H. Hoffstaetter, S. Posen, P. Quigley, and V. Veshcherevich, High current operation of the Cornell ERL superconducting rf injector cryomodule, in *Proceedings of the 3rd International Particle Accelerator Conference, New Orleans, LA, 2012*, Vol. C1205201, pp. 2378–2380.

[26] M. Liepe, D. L. Hartill, G. H. Hoffstaetter, S. Posen, P. Quigley, and V. Veshcherevich, Experience with the Cornell ERL injector SRF cryomodule during high beam current operation, in *Proceedings of the 2nd International Particle Accelerator Conference, San Sebastián, Spain* (EPS-AG, Spain, 2011), Vol. C110904, pp. 35–37.

[27] M. Liepe, S. Belomestnykh, E. Chojnacki, Z. Conway, V. Medjidzade, H. Padamsee, P. Quigley, J. Sears,

V. Shemelin, and V. Veshcherevich, SRF experience with the Cornell high-current ERL injector prototype, in *Proceedings of the 23rd Particle Accelerator Conference, Vancouver, Canada, 2009*, TU3RAI01.

[28] R. Eichhorn, B. Bullock, B. Elmore, B. Clasby, F. Furuta, Y. He, G. Hoffstaetter, M. Liepe, T. O'Connell, J. Conway, P. Quigley, D. Sabol, J. Sears, E. Smith, and V. Veshcherevich, The Cornell main linac cryomodule: A full scale, high Q accelerator module for cw application, Phys. Procedia **67**, 785 (2015).

[29] F. Furuta *et al.*, ERL main linac cryomodule cavity performance and effect of thermal cycling, in *Proceedings of the 7th International Particle Accelerator Conference (IPAC 2016), Busan, Korea, 2016* (JACoW, Geneva, Switzerland, 2016), WEPMR022.

[30] Y. He, G. H. Hoffstaetter, M. Liepe, M. Tigner, and E. N. Smith, Cryogenic distribution system for the proposed Cornell ERL main linac, in *Proceedings of the 3rd International Particle Accelerator Conference, New Orleans, LA, 2012*, Vol. C1205201, pp. 619–621.

[31] H. Luck and Ch. Trepp, Thermoacoustic oscillations in cryogenics. Part 1: Basic theory and experimental verification, Cryogenics **32**, 690 (1992).

[32] B. J. Hansen, O. Al Atassi, R. Bossert, J. Einstein-Curtis, J. Holzbauer, W. Hughes, J. Hurd, J. Kaluzny, A. Klebaner, J. Makara, Y. Pischalnikov, W. Schappert, R. Stanek, J. Theilacker, R. Wang, and M. J. White, Effects of thermal acoustic oscillations on LCLS-II cryomodule testing, IOP Conf. Ser. Mater. Sci. Eng. **278**, 012188 (2017).

[33] N. Banerjee, J. Dobbins, F. Furuta, G. Hoffstaetter, R. Kaplan, M. Liepe, P. Quigley, E. Smith, and V. Veshcherevich, Microphonics suppression in the CBETA linac cryomodules, J. Phys. Conf. Ser. **1067**, 082004 (2018).

[34] A. Neumann, W. Anders, R. Goergen, J. Knobloch, O. Kugeler, S. Belomestnykh, J. Dobbins, R. Kaplan, M. Liepe, and C. Strohman, Cw measurements of Cornell LLRF system at hobicat, in *Proceedings of the 15th Superconducting Radio Frequency Workshop (SRF '2011), Chicago, 2011* (JACoW Publishing, Geneva, Switzerland, 2011), Number 15, MOPO67.

[35] M. Liepe, S. Belomestnykh, J. Dobbins, R. Kaplan, C. Strohman, and B. Stuhl, Experience with the new digital rf control system at the CESR storage ring, in *Proceedings of the 21st Particle Accelerator Conference, Knoxville, TN, 2005* (IEEE, Piscataway, NJ, 2005), pp. 2592–2594.